Received: 19 September 2017 | Revised: 20 February 2018 | Accepted: 25 March 2018

DOI: 10.1002/hipo.22846

RESEARCH ARTICLE

WILEY

Time-varying synchronous cell ensembles during consummatory periods correlate with variable numbers of place cell spikes

Saichiro Yagi[1] | Hideyoshi Igata[1] | Yu Shikano[1] | Yuki Aoki[1] | Takuya Sasaki[1] | Yuji Ikegaya[1,2]

[1]Graduate School of Pharmaceutical Sciences, University of Tokyo, 7-3-1 Hongo Bunkyo-ku, Tokyo, 113-0033, Japan

[2]Center for Information and Neural Networks, Suita City, Osaka, 565-0871, Japan

Correspondence
Takuya Sasaki, Graduate School of Pharmaceutical Sciences, University of Tokyo, 7-3-1 Hongo, Bunkyo-ku, Tokyo, 113-0033, Japan.
Email: tsasaki@mol.f.u-tokyo.ac.jp

Funding information
Grant sponsor: Kaken-hi (17H05939 and 17H05551); Grant sponsor: Nakatomi Foundation; Grant sponsor: Suzuken Memorial Foundation

Abstract

Spike rates of a hippocampal place cell are not constant and vary even when an animal visits an identical place field with nearly identical behavior. As one potential neurophysiological source underlying place cell spiking variability, we focused on the temporally fluctuating activity states of neuronal ensembles. Spike patterns of hippocampal neurons were recorded from rats performing a linear track task. Within a single consummatory period, similar sets of neurons were more frequently recruited in synchronous firing events, whereas different synchronized firing patterns of neuronal populations tended to be identified in different consummatory periods. A linear regression analysis indicated that the time-varying activation patterns of neuronal populations during consummatory periods are correlated with the spike rates of a place cell within its place field during running. These findings suggest that place cell in-field spiking is not only triggered by static inputs that represent external environments but also strongly depends on the time-varying internal states of neuronal populations.

KEYWORDS

place cell, prediction, synchronization, trail-to-trail variability

1 | INTRODUCTION

Hippocampal pyramidal neurons specifically discharge in restricted regions of an environment, termed place cells, which are thought to embody the internal representation of a cognitive map for spatial processing (O'Keefe & Nadel, 1978). In general analyses, the spiking patterns of place cells have been characterized based on a spatial distribution of averaged spike rates computed from an entire recording session. However, a place cell emits variable numbers of action potentials every time an animal visits an identical place field (Fenton & Muller, 1998; Huxter, Burgess, & O'Keefe, 2003; Jackson & Redish, 2007).

One theory has suggested that extreme temporal variability, referred to as overdispersion, of place cell discharge may arise from a switch in active cell assemblies that correspond to multiple spatial submaps (Fenton et al., 2010; Jackson & Redish, 2007; Kelemen & Fenton, 2010). According to the multiple map theory, place cell firing variability may be minimized when animals engage in a single attentional focus to encode a behavioral context, such as when animals run in one direction on a one-dimensional linear track (Jackson & Redish, 2007). In these conditions, a certain extent of place cell spiking variability remains, as shown in Figure 1.

One of the unique neuronal dynamics that represent network states in the hippocampus is the transient synchronous reactivation of a substantial number of neurons that are typically associated with sharp-wave ripple (SWR) complexes in hippocampal local field potential (LFP) signals (Buzsaki, 1986; Buzsaki, Horvath, Urioste, Hetke, & Wise, 1992) and are thought to be essential for memory consolidation (Girardeau, Benchenane, Wiener, Buzsaki, & Zugaro, 2009; Wilson & McNaughton, 1994), spatial navigation and behavior planning (Carr, Jadhav, & Frank, 2011; Jadhav, Kemere, German, & Frank, 2012; Pfeiffer & Foster, 2013). Notably, the magnitude of the neuronal synchrony during a single SWR and neuronal population recruited in individual synchronous events is not homogeneous and varies from event to event (Csicsvari, Hirase, Mamiya, & Buzsaki, 2000; Mizuseki & Buzsaki, 2013; Ramirez-Villegas, Logothetis, & Besserve, 2015; Ylinen et al., 1995), suggesting that the neuronal network states that underlie the synchronized firing of neuronal populations continuously change over time.

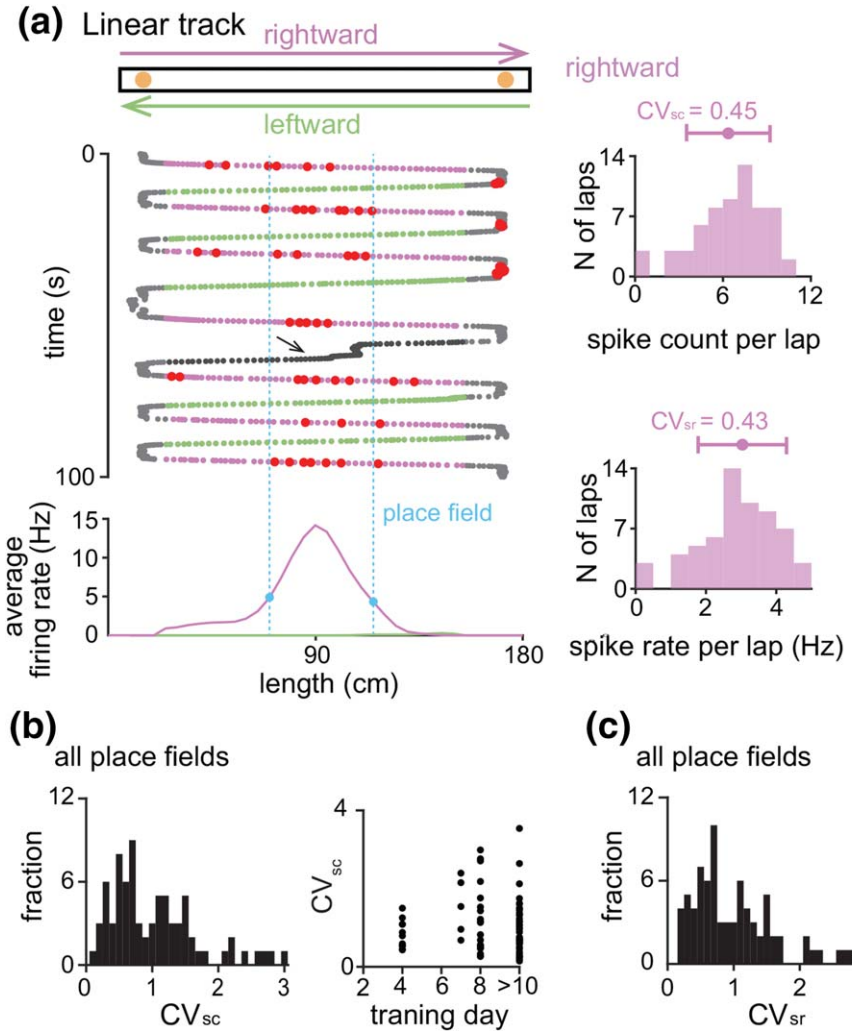

FIGURE 1 Variability of place cell spikes during unidirectional running on a linear track. (a; Top) Schematic of the linear track task. (Middle) A representative spatial firing of a CA1 place cell. Spike locations (red) were plotted on the animal's trajectory (magenta, rightward; green, leftward; gray, consummatory period). Black dots represent a lap with deceleration in the middle of the track (arrow) and were excluded from further analyses. (Bottom) Average firing-rate distribution in which the total number of spikes that occurred in a given location was normalized by the total duration that the animal spent in the location. This neuron had a place field on rightward running laps. The range of the place field was defined from the distribution as shown in the dotted blue vertical lines. (Right top) Distribution of spike counts within the place field per rightward running lap observed from an entire recording period of 10 min. Mean ± *SD* is shown on the top (CV_{sc} = 0.45). (Right bottom) Same as in the top panel but for distribution of spike rates within the same place field. CV_{sr} = 0.43. (b; Left) Summarized distribution of the CV_{sc} computed from 78 place fields from 62 place cells. (Right) Relationship between training days and CV_{sc} (r = .01, p = .90). (c) Same as in b, but for the distribution of the CV_{sr} [Color figure can be viewed at wileyonlinelibrary.com]

Together, the available evidence raises the possibility that the variable spatial spiking of place cells may be associated with the variable synchronous activity patterns of neuronal populations. In the current study, we tested this idea by analyzing the spiking patterns of hippocampal putative pyramidal cells from rats performing a linear track task. The task condition enables repeated measurements of neuronal spiking with nearly identical movement patterns (e.g., instantaneous running speed, direction of running, and reward consumption periods) and minimization of the overdispersion of place cell spiking driven by the switching of active cell assemblies as previously described (Jackson & Redish, 2007). Our analysis demonstrated that the activation patterns of hippocampal neuronal populations during consummatory periods are associated with the prospective and retrospective spatial spiking of a place cell.

2 | MATERIALS AND METHODS

2.1 | Animal ethics

Animal experimentation: This study was performed in strict accordance with the recommendations in the NIH Guide for the Care and Use of Laboratory Animals. All animals were handled according to the approval

TABLE 1 Comparison of the average *z*-scored correlation coefficients (left) and the percentages of significant laps (right) between the within-lap comparison (within) and the across-laps (across) comparison groups in all animals tested

Rat (data)	Direction	N active cells	Number of laps	Averaged *z*-score		Percentage of significant laps (%)	
				Within	Across	Within	Across
e013_670	Left	15	56	−0.06	−0.25	0.0	1.3
	Right	16	57	0.12	−0.12	6.5	7.5
e013_738	Left	12	53	1.09	0.24	35.8	31.2
	Right	12	53	0.94	−0.31	27.5	18.8
e014_639	Left	12	61	0.81	−0.42	36.8	11.7
	Right	14	53	4.77	−1.07	52.4	20.0
1	Left	10	11	0.66	0.37	17.6	20.9
	Right	12	21	0.84	−0.30	18.8	13.3
2	Left	9	34	2.99	−0.36	65.9	38.3
	Right	12	44	2.29	−0.02	50.0	30.1
3	Left	12	39	1.81	0.31	51.3	35.8
	Right	12	37	1.06	−0.07	34.2	24.3

The average *z*-scored correlation coefficients were calculated from all laps. Running patterns are separately presented for each running direction. "N active cells" represent the number of active cells defined at consummatory periods. Data were analyzed as indicated in Figure 2d

of the experimental animal ethics committee at the University of Tokyo (approval number: P29-7). All surgeries were performed under aseptic conditions and isoflurane anesthesia.

2.2 | Subjects

Three male Long Evans rats (3–12 months old) with a preoperative weight of 404–512 g were used in this study. The animals were individually housed and maintained on a 12-hr light/dark schedule with lights off at 7:00 a.m. All animals were purchased from SLC (Shizuoka, Japan). Following at least 1 week of adaptation to the laboratory, the rats were reduced to 85% of their *ad libitum* weight through limited daily feeding. Water was readily available.

2.3 | Surgical procedures

The rats were anesthetized with isoflurane gas (2%–2.5%). A craniotomy with a diameter of ~2 mm was performed using a high-speed drill, and the dura was surgically removed. Two stainless-steel screws were implanted in the bone above the frontal cortex to serve as the ground and reference electrodes. An electrode assembly that consisted of 8 independently movable tetrodes, which was created using a 3D printer (MiiCraft, Young Optics), was stereotaxically implanted above the right hippocampus (4.0 mm posterior and 2.7 mm lateral to the bregma). The electrodes were constructed from a 17-μm-wide polyimide-coated platinum-iridium (90%/10%) wire (California Fine Wire), and the electrode tips were plated with platinum to lower the electrode impedance to 150–300 kΩ at 1 kHz. The recording device was secured to the skull using stainless-steel screws and dental cement. The electrode bundle tip was lowered to the cortical surface, and the electrodes were inserted 1.0 mm into the brain at the end of the surgery. Following the surgery, each rat was individually housed in a transparent Plexiglas cage with free access to water and food for at least 3 days, followed by food deprivation to 85% of its original body weight.

2.4 | Linear track task

After surgery, the animals were trained daily for the linear track task for at least 4 days (Figure 1b and Table 1). The training was performed with the recording headstage and cable attached to the animals so that the animals could become familiar with the recording condition. All behavioral experiments occurred in the dark phase. The animal was trained to run back and forth on a linear track (180 × 9 cm with small sides rising 1.5 cm above the surface of the arm, 93 cm elevated from the floor) to obtain a constant amount of ~0.2 ml of chocolate milk reward placed at the track end during a 10-min session. This training was repeated daily for 10 min until the animal consumed the reward at least 30 times within the 10-min session. To monitor the rat's moment-to-moment position, a red LED was attached to the animal's neck, and the LED signal position was tracked at 25 Hz using a video camera located on the ceiling and sampled by a laptop computer. The rats were maintained in a rest box (43 × 25 cm) outside the field for 5–10 min before and after the task.

2.5 | Electrophysiological recordings

The rats were connected to the recording equipment via Cereplex M (Blackrock), a digitally programmable amplifier close to the rat's head.

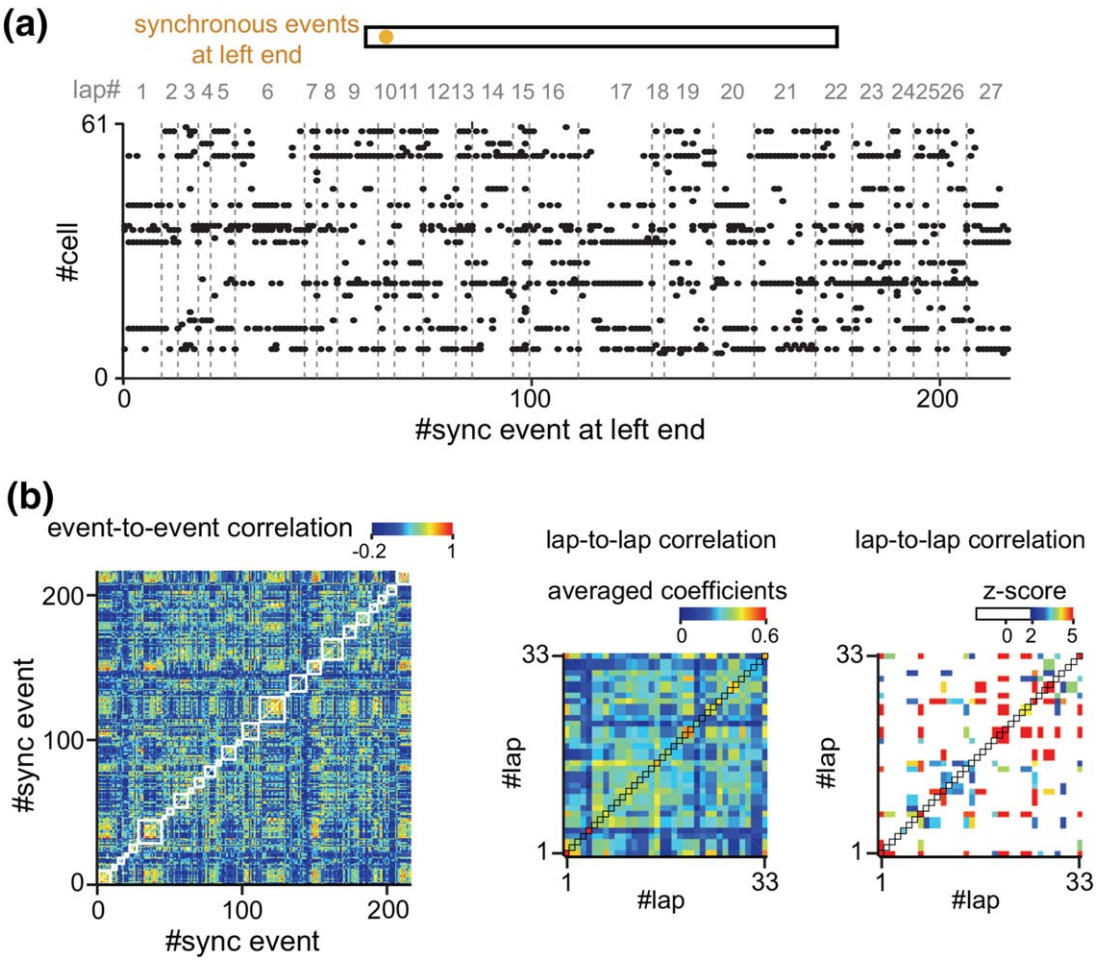

FIGURE 2 Synchronous firing activity during consummatory periods. (a) Population rasterplot of spiking patterns involved in individual synchronous events observed at the left end of the track. Individual consummatory periods are separated by gray vertical dotted lines and labeled as the lap number (#lap) on the top in gray. The data is from ec014.639. (b; Left) The event-to-event correlation matrix constructed from the rasterplot in a. Correlation coefficients computed within the same lap, termed the within-lap comparison group, are indicated by white boxes. The others outside the boxes were classified as the across-laps comparison group. (Middle) The lap-to-lap correlation matrix constructed from the event-to-event matrix. Coefficients computed in the within-lap comparison group were plotted on the diagonal line indicated by the black boxes. (Right) The *z*-scored matrix. A significant lap comparison with a *z*-score of more than 1.96 is colored. All data are summarized in Table 1 [Color figure can be viewed at wileyonlinelibrary.com]

The output of the headstage was conducted via a lightweight multiwire tether and a commutator to the Cerebus recording system (Blackrock), a data acquisition system. Electrode turning was performed while the rat was resting on a pot placed on a pedestal. Over a period of at least 2 weeks after surgery, the electrode tips were slowly advanced 25–100 μm per day for up to 20 days until spiking cells were encountered in the CA1 layer of the hippocampus, which were identified based on LFP signals and single-unit spike patterns. The tetrodes were settled into the cell layer for stable recordings over a period of several days. After confirming that stable well-separated unit activity was identified in the hippocampus and the animal reached the criterion performance, electrophysiological data during the linear track task were collected for at least 10 min. LFP recordings were sampled at 2 kHz and low-pass filtered at 500 Hz. The unit activity was amplified and bandpass filtered at 500 Hz to 6 kHz. Spike waveforms above a trigger threshold (40 μV) were time-stamped and recorded at 30 kHz for 1.6 ms.

2.6 | Histological analysis

The rats received an overdose of urethane and were intracardially perfused with 4% paraformaldehyde in phosphate-buffered saline (pH 7.4) and decapitated. To aid in the electrode track reconstruction, the electrodes were not withdrawn from the brain for at least 3 hr after the perfusion. Following dissection, the brains were fixed overnight in 4% PFA and subsequently equilibrated with a sequence of 20% sucrose and 30% sucrose in phosphate-buffered saline. Frozen coronal sections (40 μm) were cut using a microtome, and serial sections were mounted and processed for cresyl violet staining. The slices were subsequently

coverslipped with Permount. The positions of all tetrodes were confirmed by identifying the corresponding electrode tracks in the histological tissue.

2.7 | Spike sorting

Spike sorting was performed offline using the graphical cluster-cutting software Mclust (Redish, 2009). Clustering was performed manually in 2D projections of the multidimensional parameter space (i.e., comparisons between the waveform amplitudes, waveform energies, and first principal component coefficient [PC1] of the energy normalized waveform, each measured on the four channels of each tetrode). The cluster quality was measured by computing L_{ratio} and Isolation Distance (Schmitzer-Torbert, Jackson, Henze, Harris, & Redish, 2005). A cluster was considered as a cell when the L_{ratio} was less than 0.30 and Isolation distance is more than 14. An average L_{ratio} and Isolation distance were 0.18 ± 0.06 (median = 0.18) and 19.4 ± 7.9 (median = 16.2). In the same datasets, an average modified L_{ratio}, normalized by the total number of all spikes (Pfeiffer & Foster, 2013), was 0.0024 ± 0.0034 (median = 0.0013). No significant differences in L_{ratio} and Isolation distance were found between place cells and other cells (Mann-Whitney U test, $p > .05$). Cells with an average firing rate of less than 3 Hz and waveforms longer than 200 μs were considered putative excitatory cells and included in the analysis.

2.8 | Downloaded dataset

To reduce the number of animals and confirm the reproducibility of our results, we analyzed additional datasets available via the Collaborative Research in Computational Neuroscience (CRCNS) data sharing website (https://crcns.org/; for more details, refer to (Mizuseki et al., 2014)), termed "CRCNS data". The CRCNS data comprised spike trains of hippocampal pyramidal neurons recorded with multiple silicon probes from 2 rats performing a linear track task. The task condition was similar to the current experiments with the exception that the size of the track was 250×7 cm, and the reward was water (for more details, refer to Mizuseki et al., 2014). The dataset files analyzed in this study included three recording sessions, "ec013.670" (33 cells; recording duration of 20 min; 38 days after electrode implantation), "ec013.738" (39 cells; recording duration of 21 min; 41 days after electrode implantation), and "ec014.639" (61 cells; recording duration of 64 min; 36 days after electrode implantation). The criteria for dataset selection were as follows: (a) the number of simultaneously recorded neurons was more than 30, (b) the number of running laps (for definition, refer to subsequent section) was more than 50, and (c) the animals were well-trained on the task for at least 10 days. In the following analyses, we merged our datasets and the CRCNS datasets to report statistical results, unless otherwise specified.

2.9 | Analysis of spatial firing

The linear track was divided into two parts: (a) the consummatory area, a region within 14.4 and 20 cm (1/12.5 of the total track length) from both track ends in our data and the CRCNS data, respectively and (b) the running area, a track area without the consummatory area. Consummatory periods were defined as periods during which the animals were located in the consummatory area. An instantaneous speed for each frame was calculated based on the total distance traveled within a period of five frames (~200 ms) before and after the focused frame. A lap was judged as a "running lap" if the animal's instantaneous running speed exceeded 30 cm/s within the running area after departing the previous consummatory area and if the speed was maintained at more than 5 cm/s throughout the lap until reaching the opposite consummatory area. Laps that did not meet these criteria were judged as laps that included decelerating, stopping, or returning behavior and were excluded from further analyses (e.g., Figure 1a).

For each cell, an average spatial firing rate distribution with a bin size of 5 cm was computed from all running laps toward one direction. All spiking-rate distributions were smoothed by a one-dimensional convolution with a Gaussian kernel with a standard deviation of one pixel (5 cm). A place cell was defined based on the following criteria. The first criterion was that the maximum spiking rate in its average spatial spiking-rate distribution exceeded >1 Hz. The second criterion was either one of the following criteria: (a) a spiking rate in the 5 cm bin adjacent to the consummatory area was less than 20% of the maximum spiking rate or (b) the position giving the maximum spiking rate was at least 50 cm away from the 10 cm bin adjacent to the consummatory area. The second criterion was set to minimize the cases in which the spatial spiking overlapped with synchronous events in consummatory areas. In cells that met these two criteria, the range of spatial spiking, termed place field, was defined by finding the bin with the maximum spiking rate in the spatial-spiking rate distribution and then iteratively extending the field to any adjacent bins that had spiking rates of >30% of the maximum rate (an example shown in Figure 1a). The third criterion was that the length of a place field is less than 100 cm. Cells that met all of the three criteria were classified as place cells whereas non-classified cells were classified as other cells. Under these criteria, some cells had one place field with one of two directions (unidirectional place field), whereas the other cells had two place fields with both directions (bidirectional place fields). In the following analyses, bidirectional place fields from a single place cell were counted as two place fields and were separately analyzed. For each running lap, spike counts and spike rates were calculated over the period of passing the place fields in one direction. Irrespective of spatial selectivity, cells that exhibited at least one spike in more than 50% of all consummatory periods at a track end were defined as "active cells at consummatory periods". The number of active cells at consummatory periods was summarized in Table 1.

2.10 | Analysis of synchronous events

During consummatory periods, synchronous events were detected when (a) ≥30% of active cells at consummatory periods were simultaneously activated in a time window of 200 ms that was preceded by >200-ms of silence and (b) the running speed of the animals was less than 5 cm/s. The characteristics of synchronous events (e.g., the average frequency, percentage of active neurons, correspondence with SWRs) were reported based on all synchronous events.

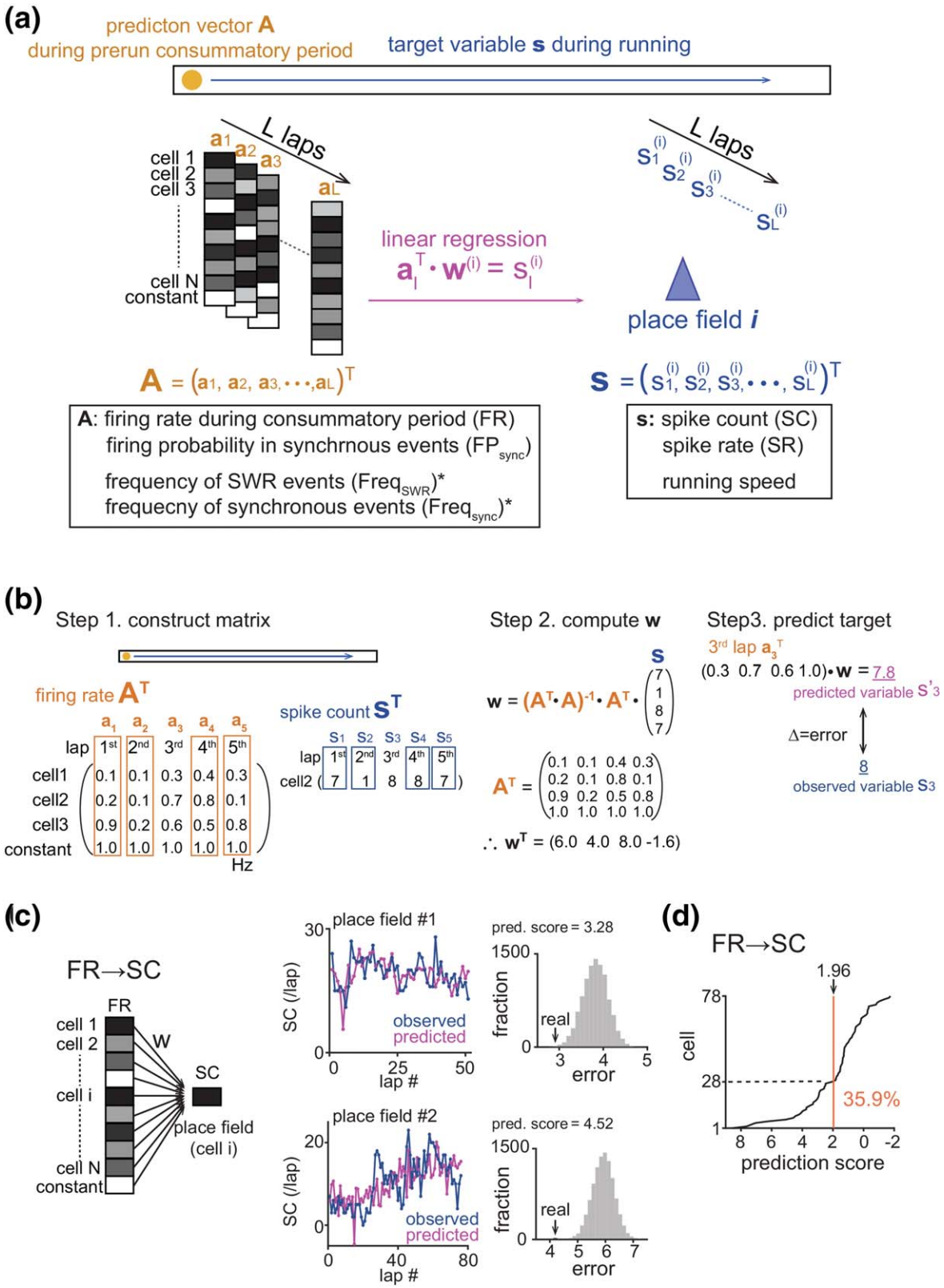
(a)
predicton vector A
during prerun consummatory period
target variable s during running
L laps
cell 1
cell 2
cell 3
cell N
constant
linear regression
place field i
A: firing rate during consummatory period (FR)
firing probability in synchrnous events (FP sync)
frequency of SWR events (Freq SWR)*
frequecny of synchronous events (Freq sync)*
s: spike count (SC)
spike rate (SR)
running speed
(b)
Step 1. construct matrix
firing rate A^T
spike count s^T
Hz
Step 2. compute w
Step3. predict target
3rd lap a3^T
(0.3 0.7 0.6 1.0)• w = 7.8
predicted variable S'3
Δ=error
8
observed variable S3
∴ w^T = (6.0 4.0 8.0 -1.6)
(c)
FR→SC
FR
W
SC
place field
(cell i)
place field #1
observed
predicted
SC (/lap)
lap #
pred. score = 3.28
fraction
real
error
place field #2
pred. score = 4.52
(d)
FR→SC
1.96
cell
35.9%
prediction score

FIGURE 3.

To quantify the similarity of the synchronous events, laps that included more than two synchronous events were specifically analyzed, as shown in Figure 2a. These synchronous events were converted to an N-dimension vector $\boldsymbol{e}$ with entries of +1 or 0 depending on whether or not the individual neurons emit an action potential in the event, respectively, where N denotes the total number of neurons. The vector series $(\boldsymbol{e}_1, \boldsymbol{e}_2, \boldsymbol{e}_3, \cdots, \boldsymbol{e}_T)$ represents a time change in active cell sets, where T denotes the total number of synchronous events. Correlation coefficients between all possible pairs of events were calculated to construct an event-to-event correlation matrix (Figure 2b, left). A lap-to-lap correlation matrix was subsequently constructed from the event-to-event matrix by calculating the average of all correlation coefficients included in each lap pair. To evaluate the significance of these averaged correlation coefficients, we applied the same analysis to randomized data wherein the temporal order of the actual synchronous events in the original data was shuffled with keeping the total numbers of synchronous events included in individual laps. This randomization was repeated 100 times, meaning that 100 surrogate lap-to-lap correlation matrices were created. At each point, a z-scored correlation coefficient of the real data was computed based on a distribution of 100 surrogate correlation coefficients (Figure 2b, right). A z-score greater than 1.96 was considered a significant coefficient.

2.11 | SWR detection

The electrode including the largest number of putative pyramidal cells identified in the spike sorting process was used for the ripple analysis. The LFP signal was bandpass filtered at 150–250 Hz, and the envelope of the filtered LFP trace was computed via Hilbert transformation (Cheng & Frank, 2008). SWR events were detected if the envelope exceeded a threshold for at least 15 ms. The frequencies of SWRs during consummatory periods were 0.42 ± 0.25 Hz and 0.20 ± 0.18 Hz at detection thresholds of three and four standard deviations (*SD*s) above the mean, respectively. In this study, we selected a threshold of three *SD*s above the mean in the analyses.

2.12 | Prediction of place cell spikes

Using linear regression analysis, we predicted a spike count of a place cell during a running period from activation patterns of neuronal ensembles during a consummatory period before running (Figures 3–5). Active cells at consummatory periods were used for a predictor vector. In the lth consummatory period at the same track end, a $(N+1)$-dimensional predictor vector was defined as a population vector $\boldsymbol{a}_l$, the N-dimensional entries of which were the average firing rate (FR) of individual activated cells during the lth consummatory period or the firing probabilities (i.e., event participation rates; FP_{sync}) of individual activated cells in synchronous events during the lth consummatory period, where N denotes the total numbers of activated cells, and the $(N+1)$th entry was set at +1 for a constant term. For a place field i, a target variable $s_l^{(i)}$ was set as a spike count (SC) or spike rate (SR) computed from an entire period of a running lap after the lth consummatory period. A linear regression function was applied to estimate a linear relationship between a series of predictor vectors, $\mathbf{A}=(\boldsymbol{a}_1, \boldsymbol{a}_2, \boldsymbol{a}_3, \ldots, \boldsymbol{a}_L)^T$, and a series of target variables, $\boldsymbol{s}^{(i)}=\left(s_1^{(i)}, s_2^{(i)}, s_3^{(i)}, \ldots, s_L^{(i)}\right)^T$, where L denotes the total numbers of consummatory events and is greater than $(N+1)$. The best $(N+1)$-dimensional weighted vector $\boldsymbol{w}^{(i)}$ was mathematically computed as follows:

$$\boldsymbol{w}^{(i)}=\mathbf{A}^{+}\boldsymbol{s}^{(i)},$$

where $\mathbf{A}^{+}=(\mathbf{A}^T\mathbf{A})^{-1}\mathbf{A}^T$.

To evaluate the predictability of the lth target variable $s_l^{(i)}$, a leave-one-out cross-validation was performed by computing $\boldsymbol{w}^{(i)}$ from the dataset without $\boldsymbol{a}_l$ and $s_l^{(i)}$. A predicted target variable $s'^{(i)}_l$ was calculated as follows:

$$s'_l(i)=\boldsymbol{a}_l^T\boldsymbol{w}^{(i)}.$$

FIGURE 3 Active cell ensembles during prerun consummatory periods predict subsequent place cell spiking. (a) Illustration of the linear regression analysis. In each lap, a predictor vector $\boldsymbol{a}$ was defined as a distribution of the firing rates (FR) or firing probabilities in synchronous events (FP_{sync}) of active cells during prerun consummatory periods. In Figure 5e,f, the predictor vector $\boldsymbol{a}$ was the frequency of SWR events ($Freq_{SWR}$) and the frequency of synchronous events ($Freq_{sync}$) during prerun consummatory periods. In these cases (indicated by asterisks), the vector had only a one-dimensional entry in addition to a constant term. A target variable $\boldsymbol{s}$ was set as the spike count (SC) or spike rate (SR) of a place field i during a running lap after each consummatory period. In Figure 5d, a target variable $\boldsymbol{s}$ was set as the animal's running period. (b) An example procedure of the linear regression analysis with a dataset from 3 cells and 5 laps. Here, the SC of cell 2 in the 3rd lap (s_3) was subject to a leave-one-out cross-validation using a dataset of the other laps (1st, 2nd, 4th, and 5th laps). Step 1: construct a series of predictor vectors, $\mathbf{A}=(\boldsymbol{a}_1, \boldsymbol{a}_2, \boldsymbol{a}_4, \boldsymbol{a}_5)$, and target variables, $\boldsymbol{s} = (s_1, s_2, s_4, s_5)$. Step 2: compute $\boldsymbol{w}$. Step 3: compute the weighted linear sum ($= a_3^T \quad \boldsymbol{w}$) as s_3. This predicted value was compared with s_3 by calculating an average absolute difference between the two variables as an error. (c; Left) A schematic of prediction in which a predictor vector $\boldsymbol{a}$ is used as a distribution of the FR of all reactivated cells during consummatory periods and a target variable $\boldsymbol{s}$ is set as the SC of a place field (FR→SC). (Middle and Right) Example analyses from two representative place fields. Prediction data were computed by repeatedly applying the cross-validation analysis in each lap. (Middle) Lap-by-lap changes in observed SCs per lap (blue) were compared with predicted SCs (magenta). (Right) An error of prediction from the real data computed from the left panel (black arrow) was compared with errors of prediction from surrogate datasets in which observed SCs were randomly shuffled across laps (gray distribution). Each shuffle was performed 10,000 times. A prediction score was computed as a negative value of a z-score defined by the surrogate distribution. (d) A cumulative distribution of the prediction score computed from the datasets in which a predictor vector $\boldsymbol{a}$ was a FR distribution and a target variable $\boldsymbol{s}$ was set as SC. Significantly predicted fractions with $p < .05$ defined by z-scores are shown below the dotted line. Median = 1.38 [Color figure can be viewed at wileyonlinelibrary.com]

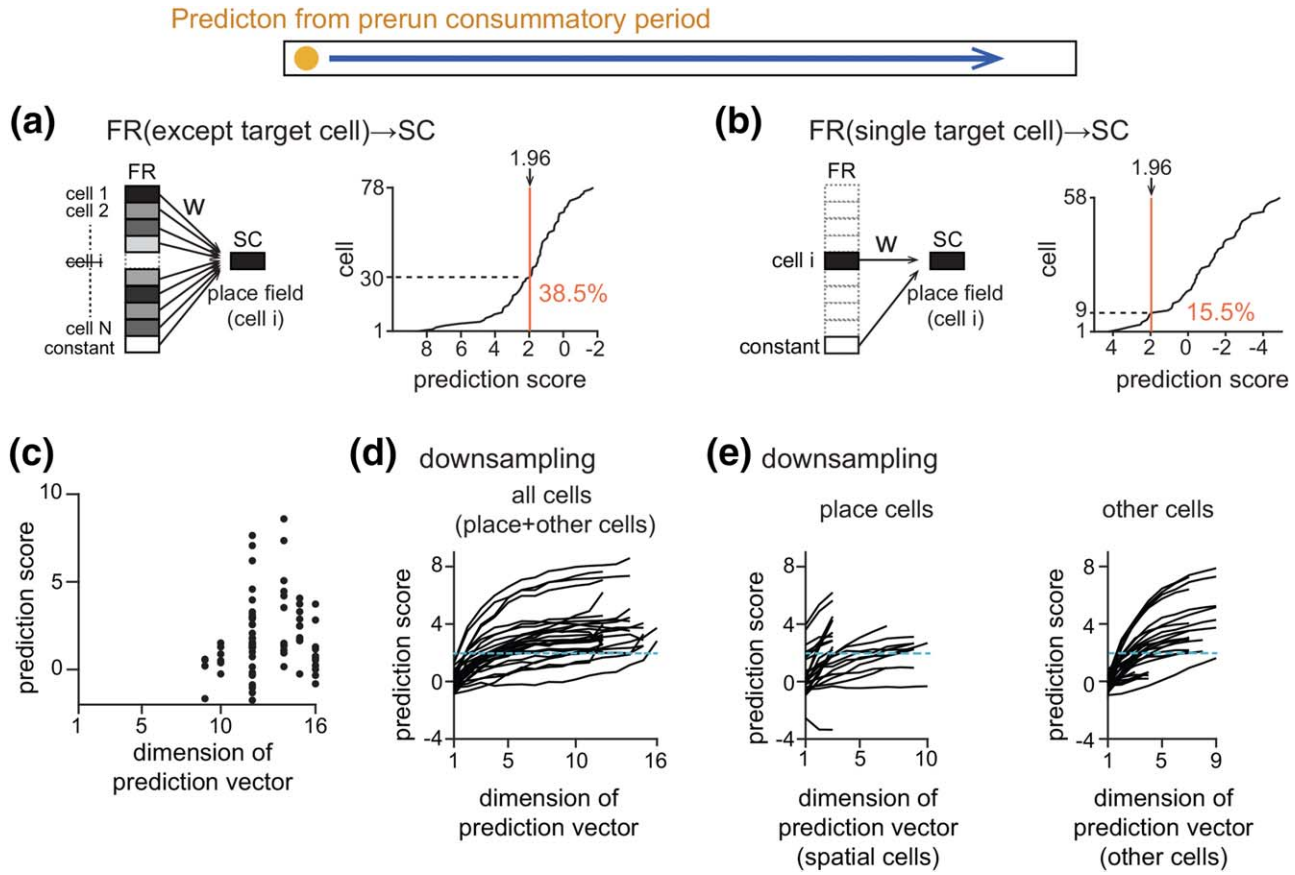

FIGURE 4 Dependence of prediction of target variables on the dimension of predictor vectors from prerun consummatory periods. (a) Same as Figure 3d with the exception that the predictor vector $\boldsymbol{a}$ was a FR distribution excluding the predicted cell, FR (except target cell). Median = 1.49. (b) Same as Figure 3d with the exception that the predictor vector $\boldsymbol{a}$ was the firing rate of the single predicted cell, termed FR (single cell). Median = −1.15. (c) No relationship between the dimension of prediction vectors and prediction scores ($r = .14$, $p = .21$). Each plot represents each predicted place field. The data correspond with that shown in Figure 3d. (d) For each place field, prediction analyses were performed using a dataset in which the dimension of prediction vectors, including both place (spatial) cells and other cells, was randomly downsampled. Each point on each line represents an average obtained from 100 randomized datasets in each place field ($n = 28$ place fields). The scores at the maximum dimension for each line correspond with the results computed from the original data. The horizontal cyan line represents prediction score = 1.96. (e) Same as d, but only place cells (left) or other cells (right) were used for prediction vectors [Color figure can be viewed at wileyonlinelibrary.com]

The same analyses were repeated for all L laps, and a series of predicted variables $\boldsymbol{s}'(i)$ for the place field i were compared with the observed variables $\boldsymbol{s}^{(i)}$ as shown in Figure 4c. The accuracy of the prediction during the timescale of an entire recording session was assessed by computing an error as an average absolute difference between the two variables, $\boldsymbol{s}^{(i)}$ and $\boldsymbol{s}'(i)$. To evaluate the significance of an error in a real data, errors were computed with the same procedures from 10,000 surrogate datasets created by shuffling the order of observed variables $\boldsymbol{s}^{(i)}$ across all running laps (Figure 3c). A zscore of the error of the real data was computed based on the distribution of the 10,000 surrogate dataset, and a prediction score for a place field was defined as a negative value of the z-score. In Figure 5e,f, the same analytical method was applied to the dataset in which the frequency of SWRs (Freq_{SWR}) and the frequency of synchronous events ($\text{Freq}_{\text{sync}}$) during a consummatory period was used as a one-dimensional entry of a predictor vector $\boldsymbol{a}$, respectively. In these cases, the predictor vector $\boldsymbol{a}$ was a 2D vector with the second entry of +1 as a constant term. In Figure 5d, a target variable $\boldsymbol{s}$ was set as the average running speed of the animal on the running area in a running lap.

2.13 | Statistics

The significance of a correlation between two variables was evaluated by computing Pearson correlation coefficients. Comparisons of two-sample data were analyzed via Mann-Whitney U test. The null hypothesis was rejected at the $p < .01$ level, unless otherwise specified. All measurements are reported as the mean ± SD and were analyzed using MATLAB.

3 | RESULTS

In this study, we simultaneously recorded a total of 20, 15, and 14 hippocampal CA1 putative pyramidal neurons from three rats performing a 10-min linear track task. In addition, we downloaded the CRCNS

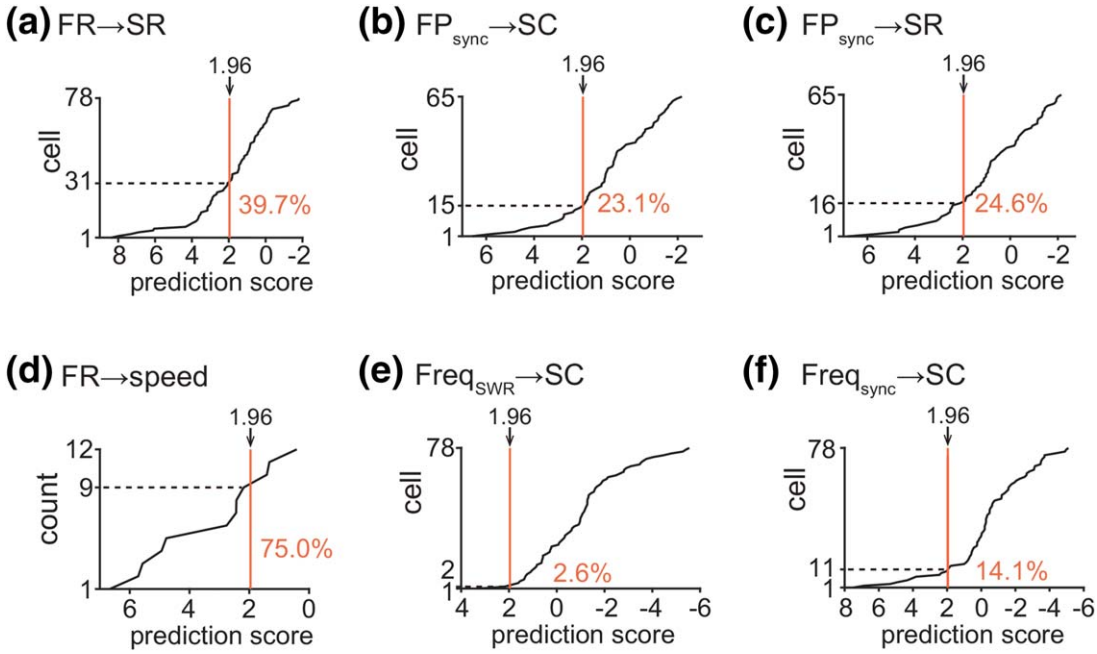

FIGURE 5 Prediction of target variables on the track by various types of predictor vectors constructed from prerun consummatory periods. (a–c) Same as Figure 3d with the exception that the target variable ***s*** was set as the SR of a single place field (a) or a predictor vector ***a*** was a FP_{sync} distribution (b and c). (a, Median = 1.45; b, Median = 0.73; c, Median = 0.85). (d) Same as Figure 3d with the exception that the target variable ***s*** was the animal's running speed. Median = 2.60. The count on the *y*-axis means that two running directions were obtained from six sessions, meaning a total of 12 running directions. (e and f) Same as Figure 3d with the exception that the predictor vector ***a*** was the frequency of SWRs ($Freq_{SWR}$) or synchronous events ($Freq_{sync}$) during consummatory periods. (e, Median = −1.00; f, Median = −0.31) [Color figure can be viewed at wileyonlinelibrary.com]

datasets, which included three sessions from two rats. Overall, we analyzed the spike patterns of 186 putative pyramidal neurons in the dorsal hippocampal CA1 region of five rats performing six sessions of a linear track task. On average, one recording session included 51 ± 14 running laps per session. Of 62 place cells identified, 46 (74.2%) cells had unidirectional place fields depending on the movement direction, whereas 16 (25.8%) cells had bidirectional place fields independent of the movement direction. Here, the bidirectional place fields of a single place cell were counted as two place fields, leading to a total of 78 place fields analyzed.

An example spike pattern in a CA1 place cell is shown in Figure 1a. This neuron had a place field during running laps toward a rightward direction, with variable spike count every lap, ranging from 0 to 16 spikes/lap (mean = 6.4 spikes/lap; *SD* = 2.8 spikes/lap; coefficient of variation of the spike count (CV_{sc}) = 0.45). The distribution of the CV_{sc} obtained from all 78 place fields is summarized in Figure 1b left; the averaged CV_{sc} was 1.05 ± 0.72, ranging from 0.15 to 3.5 with a median of 0.85. The CV_{sc} was not dependent on the number of training days ($r = .01$, $p = .90$; Figure 1b, right).

Based on the following observations, we ruled out the concern that the variability of spike counts could be simply explained by the variability of the lap (sampling) duration: (a) the distribution of the CV of the spike rate (CV_{sr}) in which a spike count per lap was normalized by the duration of the corresponding running lap (Figure 1c; CV_{sr} = 1.05 ± 0.73, ranging from 0.18 to 3.9 with a median of 0.83) was not significantly different from that of the CV_{sc} as shown in Figure 1b ($D_{max} = 0.051$, $p = .99$, Kolmogorov-Smirnov test); (b) the average CV of the duration (CV_{dur}) of one running lap was 0.24 ± 0.14 ($n = 6$ sessions from 5 animals), which was considerably lower than that of the CV_{sc} ($z = 3.60$, $p = 3.1 \times 10^{-4}$, Wilcoxon rank-sum test).

We subsequently focused on synchronized activation of neuronal populations generated within hundreds of milliseconds, which were typically linked to SWRs (Csicsvari et al., 2000; Ylinen et al., 1995). Here, we identified "synchronous events (sync events)" as brief increases in the spike density during consummatory periods. In one consummatory period with an average duration of 10.0 ± 3.3 s, the average frequency of synchronous events was 0.6 ± 0.4 Hz, meaning that one consummatory period included 6.5 ± 4.4 synchronous events. During the same consummatory period, the average frequency of detected SWRs was 0.42 ± 0.25 Hz, meaning that one consummatory period included 4.7 ± 3.5 SWRs. On average, a single SWR included 3.9 ± 2.3 firing cells (9.7% ± 6.9% of all recorded cells), and 15.6% ± 8.6% of SWRs corresponded to synchronous events within a time window of 200 ms. In this study, we did not further analyze the sequential order of spikes within synchronous events because of the limitation of the sample size. During these synchronous events, other cells, in addition to spatial cells, were also activated together. Out of 3,414 ± 1,689 spikes involved in all synchronized events in one session, 37.1% ± 14.5% of the spikes were derived from other cells. Here, both spatial and other active cell ensembles are considered to cooperatively represent entire network activity states.

To assess how network states change over time, we plotted all firing patterns involved in synchronous events detected at the same track end (Figure 2a). Here, laps with less than three synchronous events were excluded from the analyses. Individual consummatory periods, labeled as lap#, contained different numbers of synchronous events as classified by dotted vertical lines. Based on this rasterplot, Pearson correlation coefficients of vectorized population spikes were computed between all pairs of synchronized events, which were summarized as an event-to-event correlation matrix (Figure 2b, left). In the matrix, the correlation coefficients computed within the same laps were enclosed by white boxes along the diagonal line, termed the within-lap comparison group, whereas others outside the boxes were termed the across-laps comparison group. The event-to-event matrix was converted to a lap-to-lap correlation matrix by calculating an average correlation coefficient in each lap pair (Figure 2b, middle). The lap-to-lap correlation matrix was subsequently converted to a *z*-scored correlation matrix using 100 surrogate datasets (Figure 2b, right; for more details, refer to Section 2). In Figure 2b right, 52.4% and 20.0% of the *z*-scored correlation coefficients were more than 1.96, termed significant coefficients, in the within-lap comparison and across-laps comparison groups, respectively. The same analysis was applied to all animals, as summarized in Table 1. On average, 33.1% ± 19.9% of laps had significant coefficients in the within-lap comparison, demonstrating that some, but not all, consummatory periods had a higher likelihood to contain similar sets of active neurons in synchronous events, compared with the surrogate datasets. The average *z*-sccore in the within-lap comparison group was significantly larger than that in the across-laps comparison group ($z = 3.72$, $p = 1.9 \times 10^{-4}$, Mann-Whitney *U* test), demonstrating that the within-lap comparison group tended to contain more correlated synchronous events, compared with the across-laps comparison group and that different cell ensembles are more likely recruited in different consummatory periods. However, there were a small fraction (21.1% ± 11.4%) of the correlation coefficients identified as significant coefficients even in the across-laps comparison group (Table 1), as shown in some examples in Figure 2b right (e.g., lap#1 vs. lap#4, lap#6 vs. lap#10). This result demonstrates that some different laps could share similar patterns of active neuronal ensembles.

We next tested whether temporally fluctuating ensemble patterns of hippocampal cell activation might correlate with the spatial spiking of individual place cells. A predictor vector $\boldsymbol{a}$ was defined as the distribution of the firing rates (FR) of all activated cells, including a predicted cell, or the firing probabilities in synchronous events (FP_{sync}) during prerun consummatory periods, and a target variable $\boldsymbol{s}$ was set as a spike count (SC) or a spike rate (SR) of a single place cell during running after the consummatory periods (Figure 3a). For each place field, a vector of weighted coefficients $\boldsymbol{w}$ was computed so that the weighted linear sum s' ($= \boldsymbol{a}^T\boldsymbol{w}$) was fitted against $\boldsymbol{s}$ of the cell (a simple example shown in Figure 3b; for more details, refer to Section 2). Figure 3c shows a prediction result from two example cells in the case in which a predictor vector $\boldsymbol{a}$ was defined as FR and a target variable $\boldsymbol{s}$ was set as SC (termed FR→SC). In each lap, a leave-one-out cross-validation analysis was applied to examine the predictability of the target variable. The predictability was evaluated by computing an error from a series of an observed target variable $\boldsymbol{s}$ and a predicted variable $\boldsymbol{s'}$. Next, to assess the significance of the real data, same analyses were applied to 10,000 surrogate datasets. A *z*-score of the real data was obtained from the surrogate distribution and a prediction score was defined as a negative value of the *z*-score. Of 78 place fields tested, 35.9% of the fields had a significantly positive prediction score of more than 1.96 at a significance level of $p < .05$ (Figure 3d).

This proportion was similar when the predicted single cell was excluded from a FR distribution of all activated cells for constructing a predictor vector $\boldsymbol{a}$, showing that prediction vectors from other cells are sufficient to predict spike counts of a target cell (Figure 4a, FR [except target cell]→SC). In contrast, This proportion was reduced to 15.5% (9 of 58 place fields of activated cells) in the case in which the FR of the predicted single cell alone was used as a predictor vector $\boldsymbol{a}$ (Figure 4b, FR [single target cell]→SC), showing that a firing rate of a single cell alone during consummatory periods is not sufficient to predict in-field firing rates in most of place cells. As the number of active cells included in prediction vectors differed across samples, prediction results may be accounted for by dimensions of prediction vectors. We tested this possibility by plotting prediction scores against the dimension of prediction vectors but found no significant correlation between them ($r = .14$, $p = .21$), at least in our original datasets with a dimension ranging from 9 to 16 (Figure 4c). We next analyzed how increased dimension of prediction vectors (i.e., higher number of active cells) contributes to improved predictability in individual datasets. To this end, firing-rate distributions used for prediction vectors were downsampled by randomly excluding cells so that the dimension of a prediction vector was reduced to a lower dimension. For each lowered dimension, prediction scores from 100 surrogates were computed. In Figure 4d, we plotted prediction results from downsampled data for place fields that exhibited significantly positive prediction scores in the original datasets ($n = 28$ place fields). Each line represents each place field showing an average prediction score computed from 100 randomized datasets. When the dimension of prediction vectors was reduced to 7, significant decreases in prediction scores were detected compared with those from prediction vectors with the maximum dimension ($z = 2.19$, $p = .029$, Mann-Whitney *U* test), and the proportions of cells exhibiting significantly positive prediction scores were reduced to 78.6% (22 out of 28 cells; Figure 4d). These results demonstrate that firing-rate distributions of at least eight or more cells during consummatory periods were required to predict place cell firing at the same level to the original data. When the dimension of prediction vectors was reduced to six and three, the proportions of cells exhibited significantly positive prediction scores were reduced to 75.0% (21 out of 28 cells) and 32.1% (9 out of 28 cells), respectively.

We examined whether spatial selectivity of cells may contribute to increased predictability by separately performing analyses for other cells (Figure 4e). When prediction vectors were specifically constructed from other cells, the dimension of prediction vectors was 6.4 ± 0.4 (ranging from 3 to 9) and the proportions of cells that exhibited significantly positive prediction scores was 71.4% (20 out of 28 cells), which was almost comparable to those from the downsampled datasets with a dimension of six including both place cells and other cells. When the dimension of these vectors was downsampled to three, the proportions

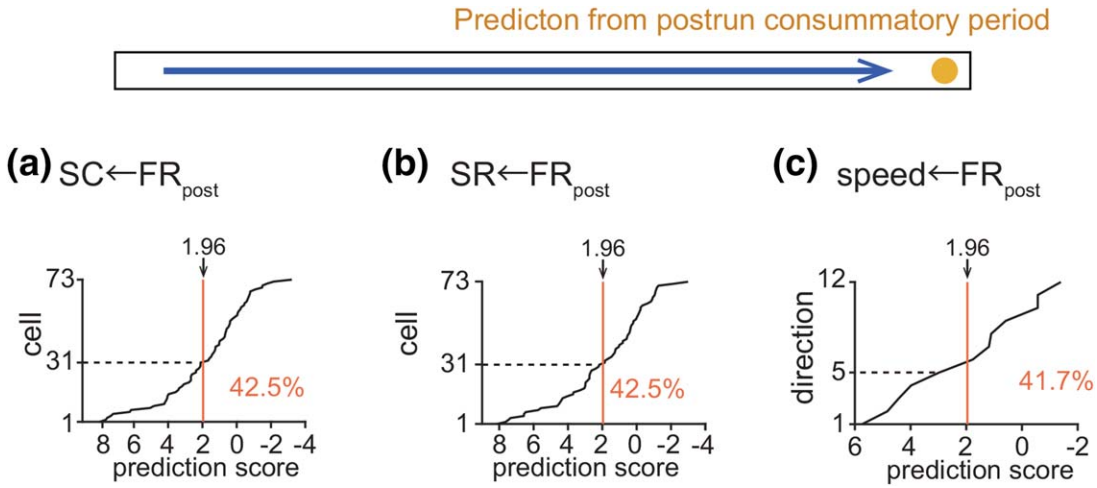

FIGURE 6 Prediction of target variables on the track from predictor vectors of a FR distribution at postrun consummatory periods. (a) A cumulative distribution of the prediction score computed from the datasets in which a predictor vector ***a*** was a FR distribution during postrun consummatory periods and a target variable ***s*** was set as a SC during running. Significantly predicted fractions with $p < .05$ defined by *z*-scores are shown below the dotted line. Median = 1.28. (b) Same as in a, but a target variable ***s*** was SR. Median = 1.28. (c) Same as in A, but a target variable ***s*** was running speed. Median = 1.48 [Color figure can be viewed at wileyonlinelibrary.com]

of cells that exhibited significantly positive prediction scores was reduced to 39.3% (11 out of 28 cells; Figure 4e, right), which was almost comparable to those from the downsampled datasets with a dimension of three including both place cells and other cells (Figure 4d). The result suggests no pronounced effects of spatial selectivity on the predictability. The same comparison was not applied to datasets with place cells due to the limited number of cells (Figure 4e, left).

The same linear regression analysis was applied to test whether other variables were predicted and other prediction vectors were used for our prediction as shown in Figure 5. Similar to the FR→SC results presented in Figure 3d, 39.7% of the place fields exhibited significantly positive prediction scores when SR was set as a target variable ***s*** (Figure 5a, FR→SR), and 23.1% or 24.6% of the place fields exhibited significantly positive prediction scores when FP_{sync} was used as a predictor vector ***a*** and SC or SR were set as a target variable ***s***, respectively (Figure 5b, FP_{sync}→SC; Figure 5c, FP_{sync}→SR). Using the same regression analysis, the average running speed of the animals on the track was predicted from the weighted linear sum of the FR-based predictor vector ***a*** in 75.0% of the datasets (Figure 5d, $n = 12$ running directions from six sessions), demonstrating that the firing patterns of neuronal ensembles during a consummatory period were linked to the subsequent running behavior. When the frequency of SWRs ($Freq_{SWR}$) and the frequency of synchronous events ($Freq_{sync}$) during a consummatory period were set as a 1D entry of a predictor vector ***a***, 2.6% and 14.1% of the place fields had a significant prediction score (Figure 5e,f), demonstrating that the frequency of synchronization of neuronal ensembles alone was less predictive than the firing patterns of neuronal ensembles for subsequent place cell firing.

The same linear regression analysis was applied to test whether a predictor vector ***a*** at postrun entire consummatory periods are associated with spike patterns of the same sets of cells at running before the consummatory periods (Figure 6). Similar to prerun consummatory periods, predictor vectors at postrun consummatory periods could predict SC, SR, and running speed on the track with approximately similar success rates (Figure 6a–c). Taken together with the results of Figures 4 and 5, these data demonstrate that there are sustained periods for place cell spikes that correlates with firing patterns of consummatory periods before and after running on the track.

4 | DISCUSSION

In this study, we analyzed the lap-to-lap firing variability of hippocampal neurons during unidirectional running in a linear track task, a condition that is assumed to contain minimal switching of the multiple spatial submap and to minimize overdispersion of the place cell discharge (Jackson & Redish, 2007). As one potential neurophysiological source underlying the firing variability, we focused on the temporal fluctuation of the synchronous activity of neuronal ensembles. Similar to spatial firing during running, the synchronous activation patterns of neuronal populations during consummatory periods varied from lap-to-lap. Our linear regression analysis demonstrated that the lap-to-lap changes in the neuronal activation patterns during a consummatory period were associated with fluctuating firing rates of place cells during running immediately after the consummatory period. These results demonstrate that the spatial firing intensity of a place cell is closely linked to the internally fluctuating activity states of neuronal networks.

As reported in previous studies, the magnitude of SWRs and the percentage of active neurons in SWR-induced synchrony are considerably variable (Csicsvari et al., 2000; Mizuseki & Buzsaki, 2013; Ramirez-Villegas et al., 2015; Ylinen et al., 1995). Our study extended these findings by showing that similar sets of neurons more preferentially participated in synchronous events within a single consummatory period, and different ensemble patterns are more likely recruited in different laps (Figure 2). Notably, different consummatory periods share

similar synchronous events, implying that active hippocampal neuronal ensembles continuously drift across multiple network states, referred to as attractor-like dynamics (McNaughton, Battaglia, Jensen, Moser, & Moser, 2006; Wills, Lever, Cacucci, Burgess, & O'Keefe, 2005). Several cellular mechanisms that underlie these network dynamics are considered, including temporal changes in the internal conductance within a single neuron, input correlations, and widespread synchronization. The other potential mechanism may include probabilistic interplay between cortical and subcortical systems. A recent study by (Ambrose, Pfeiffer, & Foster, 2016) has shown that the frequency of reverse replays in a linear track is highly sensitive to changes in reward contingency, which may represent an internal change in cognitive processing, such as an expectation of the reward magnitude and motivation for the task, presumably as a result of changes in the levels of neuromodulators, such as dopaminergic signals (McNamara, Tejero-Cantero, Trouche, Campo-Urriza, & Dupret, 2014). Our study used a constant amount of reward throughout the task; however, temporally fluctuating synchronized neuronal ensembles might reflect subtle fluctuations in the animal's level of attentional focus or the degree of task engagement.

The neurophysiological roles of the temporally fluctuating neuronal signals in the hippocampal system remain to be identified; however, they may represent a potential neural substrate to enrich brain functions. For example, they may serve to enhance the variability of the encoding of identical contexts and integrate novel information onto preexisting cognitive maps when animals are required to adapt to newly emerging contexts. An alternative role might be that fluctuating neuronal activity occasionally yields unexpected outcomes, which might be useful for linking independent experiences or imagining novel ideas. In all scenarios, a lower fidelity of neuronal activity would be more appropriate to increase the capability of information processing. From this perspective, the hippocampal circuit may be understood as a neural framework not only to stably represent the external world but also to flexibly build novel encoding patterns in the brain.

ACKNOWLEDGMENTS

We thank Dr. Kenji Mizuseki for the valuable comments on a previous version of this manuscript. The authors declare no competing financial interests.

AUTHOR CONTRIBUTIONS

T. S. designed the work, S. Y., H. I., Y. S., and Y. A. acquired electrophysiological data, S. Y. and H. I. performed analysis. Y. I. provided analytical idea and supervised the project. S. Y. and T. S. prepared all figures. T. S. wrote the main manuscript text and all authors reviewed the main manuscript text.

ORCID

Takuya Sasaki http://orcid.org/0000-0001-8890-7691

REFERENCES

Ambrose, R. E., Pfeiffer, B. E., & Foster, D. J. (2016). Reverse replay of hippocampal place cells is uniquely modulated by changing reward. *Neuron*, *91*(5), 1124–1136.

Buzsaki, G. (1986). Hippocampal sharp waves: Their origin and significance. *Brain Research*, *398*(2), 242–252.

Buzsaki, G., Horvath, Z., Urioste, R., Hetke, J., & Wise, K. (1992). High-frequency network oscillation in the hippocampus. *Science (New York, N.Y.)*, *256*(5059), 1025–1027.

Carr, M. F., Jadhav, S. P., & Frank, L. M. (2011). Hippocampal replay in the awake state: A potential substrate for memory consolidation and retrieval. *Nature Neuroscience*, *14*(2), 147–153.

Cheng, S., & Frank, L. M. (2008). New experiences enhance coordinated neural activity in the hippocampus. *Neuron*, *57*(2), 303–313.

Csicsvari, J., Hirase, H., Mamiya, A., & Buzsaki, G. (2000). Ensemble patterns of hippocampal CA3-CA1 neurons during sharp wave-associated population events. *Neuron*, *28*(2), 585–594.

Fenton, A. A., Lytton, W. W., Barry, J. M., Lenck-Santini, P. P., Zinyuk, L. E., Kubik, S., . . . Olypher, A. V. (2010). Attention-like modulation of hippocampus place cell discharge. *The Journal of Neuroscience*, *30*(13), 4613–4625.

Fenton, A. A., & Muller, R. U. (1998). Place cell discharge is extremely variable during individual passes of the rat through the firing field. *Proceedings of the National Academy of Sciences of the United States of America*, *95*(6), 3182–3187.

Girardeau, G., Benchenane, K., Wiener, S. I., Buzsaki, G., & Zugaro, M. B. (2009). Selective suppression of hippocampal ripples impairs spatial memory. *Nature Neuroscience*, *12*(10), 1222–1223.

Huxter, J., Burgess, N., & O'Keefe, J. (2003). Independent rate and temporal coding in hippocampal pyramidal cells. *Nature*, *425*(6960), 828–832.

Jackson, J., & Redish, A. D. (2007). Network dynamics of hippocampal cell-assemblies resemble multiple spatial maps within single tasks. *Hippocampus*, *17*(12), 1209–1229.

Jadhav, S. P., Kemere, C., German, P. W., & Frank, L. M. (2012). Awake hippocampal sharp-wave ripples support spatial memory. *Science*, *336*(6087), 1454–1458.

Kelemen, E., & Fenton, A. A. (2010). Dynamic grouping of hippocampal neural activity during cognitive control of two spatial frames. *PLoS Biology*, *8*(6), e1000403.

McNamara, C. G., Tejero-Cantero, A., Trouche, S., Campo-Urriza, N., & Dupret, D. (2014). Dopaminergic neurons promote hippocampal reactivation and spatial memory persistence. *Nature Neuroscience*, *17*(12), 1658–1660.

McNaughton, B. L., Battaglia, F. P., Jensen, O., Moser, E. I., & Moser, M. B. (2006). Path integration and the neural basis of the 'cognitive map'. *Nature Reviews Neuroscience*, *7*(8), 663–678.

Mizuseki, K., & Buzsaki, G. (2013). Preconfigured, skewed distribution of firing rates in the hippocampus and entorhinal cortex. *Cell Reports*, *4*(5), 1010–1021.

Mizuseki, K., Diba, K., Pastalkova, E., Teeters, J., Sirota, A., & Buzsaki, G. (2014). Neurosharing: Large-scale data sets (spike, LFP) recorded from the hippocampal-entorhinal system in behaving rats. *F1000Research*, *3*, 98.

O'Keefe, J., & Nadel, L. (1978). *The hippocampus as a cognitive map*. Oxford, UK: Oxford University Press.

Pfeiffer, B. E., & Foster, D. J. (2013). Hippocampal place-cell sequences depict future paths to remembered goals. *Nature*, *497*(7447), 74–79.

Ramirez-Villegas, J. F., Logothetis, N. K., & Besserve, M. (2015). Diversity of sharp-wave-ripple LFP signatures reveals differentiated brain-wide dynamical events. *Proceedings of the National Academy of Sciences*, *112*(46), E6379–E6387.

Redish, A. D. (2009). *MClust 3.5*, *free-ware spike sorting*. Minneapolis, MN: University of Minnesota. Available at http://redishlab.neuroscience.umn.edu/MClust/MClust.html.

Schmitzer-Torbert, N. 1., Jackson, J., Henze, D., Harris, K., & Redish, A. D. (2005). Quantitative measures of cluster quality for use in extracellular recordings. *Neuroscience*, *131*(1), 1–11.

Wills, T. J., Lever, C., Cacucci, F., Burgess, N., & O'Keefe, J. (2005). Attractor dynamics in the hippocampal representation of the local environment. *Science*, *308*(5723), 873–876.

Wilson, M. A., & McNaughton, B. L. (1994). Reactivation of hippocampal ensemble memories during sleep. *Science (New York, N.Y.)*, *265*(5172), 676–679.

Ylinen, A., Bragin, A., Nadasdy, Z., Jando, G., Szabo, I., Sik, A., & Buzsaki, G. (1995). Sharp wave-associated high-frequency oscillation (200 Hz) in the intact hippocampus: Network and intracellular mechanisms. *The Journal of Neuroscience*, *15*(1), 30–46.

How to cite this article: Yagi S, Igata H, Shikano Y, Aoki Y, Sasaki T, Ikegaya Y. Time-varying synchronous cell ensembles during consummatory periods correlate with variable numbers of place cell spikes. *Hippocampus*. 2018;28:471–483. https://doi.org/10.1002/hipo.22846